

Article

Effect of Feedstock Powder Intrinsic Characteristics on the Tribological Behavior of Inductively Remelted NiCrBSi Flame-Sprayed Coatings

Roxana Muntean ¹, Petru-Cristian Vălean ¹, Norbert Kazamer ^{2,*}, Ion-Dragoș Uțu ¹, Gabriela Mărginean ³ and Viorel Aurel Șerban ¹

¹ Materials and Manufacturing Engineering Department, Politehnica University of Timișoara, Piața Victoriei 2, 300006 Timișoara, Romania; roxana.muntean@upt.ro (R.M.); petru.valean@student.upt.ro (P.-C.V.); dragos.utu@upt.ro (I.-D.U.); viorel.serban@upt.ro (V.A.Ș.)

² Westphalian Energy Institute, Westphalian University of Applied Sciences Gelsenkirchen Bocholt Recklinghausen, Neidenburgerstr. 43, 45897 Gelsenkirchen, Germany

³ Institute of Mechanical Engineering, Westphalian University of Applied Sciences Gelsenkirchen Bocholt Recklinghausen, Neidenburgerstr. 43, 45897 Gelsenkirchen, Germany; gabriela.marginean@w-hs.de

* Correspondence: norbert.kazamer@w-hs.de

Abstract: Ni-based alloys are among the materials of choice in developing high-quality coatings for ambient and high-temperature applications that require protection against intense wear and corrosion. The current study aims to develop and characterize NiCrBSi coatings with high wear resistance and improved adhesion to the substrate. Starting with nickel-based feedstock powders, thermally sprayed coatings were initially fabricated. Prior to deposition, the powders were characterized in terms of microstructure, particle size, chemical composition, flowability, and density. For comparison, three types of powders with different chemical compositions and characteristics were deposited onto a 1.7227 tempered steel substrate using oxyacetylene flame spraying, and subsequently, the coatings were inductively remelted. Ball-on-disc sliding wear testing was chosen to investigate the tribological properties of both the as-sprayed and induction-remelted coatings. The results reveal that, in the case of as-sprayed coatings, the main wear mechanisms were abrasive, independent of powder chemical composition, and correlated with intense wear losses due to the poor intersplat cohesion typical of flame-sprayed coatings. The remelting treatment improved the performance of the coatings in terms of wear compared to that of the as-sprayed ones, and the density and lower porosity achieved during the induction post-treatment had a significant positive role in this behavior.

Keywords: NiCrBSi coatings; flame spraying; induction remelting; wear resistance



Citation: Muntean, R.; Vălean, P.-C.; Kazamer, N.; Uțu, I.-D.; Mărginean, G.; Șerban, V.A. Effect of Feedstock Powder Intrinsic Characteristics on the Tribological Behavior of Inductively Remelted NiCrBSi Flame-Sprayed Coatings. *Lubricants*

2023, 11, 363. <https://doi.org/10.3390/lubricants11090363>

Received: 31 July 2023

Revised: 23 August 2023

Accepted: 24 August 2023

Published: 26 August 2023



Copyright: © 2023 by the authors. Licensee MDPI, Basel, Switzerland. This article is an open access article distributed under the terms and conditions of the Creative Commons Attribution (CC BY) license (<https://creativecommons.org/licenses/by/4.0/>).

1. Introduction

Thermal spraying, known as a popular solution for replacing the hard chromium plating process, is currently applied to enhance products' lifetimes by ensuring wear and corrosion protection and to restore components that have deviated from their nominal sizes by different degradation mechanisms [1]. The greatest advantage of this process is that a large variety of materials can be employed to obtain coatings; theoretically, any material that does not decompose at its melting point can be used in the process [2]. Different coating materials such as cobalt-, iron-, and nickel-based alloys with or without hard carbide particles (WC and CrC) are frequently used in gas turbines, steam turbines, and aerospace engines to enhance wear and corrosion resistance [3,4]. Among them, the NiCrBSi system is widely used for tribological applications, specifically to boost the working lifetime of components that are subjected to wear [3,5]. The Ni matrix assures high ductility and oxidation resistance, Cr further enhances the wear and corrosion behavior and enables the formation of carbides and borides [5], and B and Si suppress the melting temperature

of the alloy due to the eutectic reaction, consequently forming a hard precipitate [6]. The presence of such elements promotes wettability and deoxidation, assuring the self-fluxing character of the powders during the remelting process [7]. Moreover, these elements reduce the frequency of unmelted particles occurrence after the deposition or the post-heat treatment [8,9], and C enables the creation of carbides, increasing the hardness and wear resistance of the coatings [10]. Although NiCrBSi-based coatings exhibit great behavior in tribological applications, the production rate growth in different manufacturing industries has gradually accelerated an increase in the wear degree of components [11]. Consequently, a further enhancement of the coating's wear resistance is currently required. This can be achieved either with the addition of hard reinforcing particles like WC [12], SiC [13], or Cr₃C₂ [14] in the NiCrBSi matrix by creating a composite coating, or by applying a post-processing treatment after the deposition process [5,15–17].

Offering high spraying rates (1–9 kg h⁻¹) and a wide range of coating thicknesses starting from 30 μm [18] up to several mm depending on the initial feedstock powder, thermal spraying is known to be one of the most versatile deposition methods [2]. Compared with other conventional coating processes like chemical vapor deposition, physical vapor deposition, or galvanizing, thermal spraying enables better coating of complex geometries, with tailored porosity and phase composition [19]. Among all the flame-deposition techniques, the cheapest and the most effective one is oxyacetylene powder flame deposition. This technique uses the heat from the combustion of a fuel gas (acetylene) mixed with oxygen to melt the coating material, initially in the form of powder, which is then propelled towards a substrate. Flame spraying is generally used where a cost-effective thermal spray coating is necessary but lower quality can be tolerated. According to the literature, it is known that the coatings obtained by this process consist of several layers with a lamellar structure, very high porosity, and an imminent threat of delamination [20]. These typical structural issues and imperfect lamella cohesion are not desired, as they significantly affect the corrosion behavior of the applied coatings. Furthermore, another major disadvantage is that at the interface, the particles show a mechanical anchorage to the substrate and present a high risk of exfoliation upon exposure to external forces, providing poor wear protection. In these circumstances, for better performance, it is required to subject the coatings to different surface post-treatment procedures to improve density, eliminate the splat boundaries, reduce internal stresses, and mitigate delamination risk. According to J.R. Davis [2], there are different methods to improve the quality of the resulting flame-sprayed coatings, either by applying physicochemical, mechanical, or thermal post-treatments. Surface remelting is considered an important part of the thermal process used to improve the functional properties of the surface of compact materials or coatings fabricated by different technologies. The most common methods are laser [15], electron beam [21], and induction melting [17]. Several studies have shown that a subsequent heat treatment or coating remelting can improve the wear properties and adhesion strength of the coating [9,15]. NiCrBSi alloys are among the materials that considerably benefit from the remelting process. The particular chemical composition makes the alloy easy to remelt, specifically due to the content of temperature suppressant elements. Ni-based coatings are frequently remelted using flame during or after thermal spraying [16]. Another option, induction remelting, is a method of heating metallic materials by electromagnetic induction. The process is based on the effect of high-frequency currents induced to flow to the surface of the conducting parts at a depth dependent on the frequency and duration of the applied current. The passage of current through the heating inductor generates a very intense and fast magnetic field in the space of the working coil. The workpiece to be heated is placed inside this intense alternating magnetic field [22].

Furthermore, the tribological properties of flame-sprayed coatings are mainly influenced by the parameters of the technological deposition process and post-treatment, but also by the powders' chemical composition, more specifically the concentrations of chemical elements in the feedstock powder, the size of the particles [23], the flowability that enables a high packing density [24], or the temperature of the substrate during deposition [25].

However, only a few studies have focused on the issues regarding the effect of chemical element concentrations in the NiCrBSi feedstock powder on the wear behavior of the resulting coatings [25,26].

In the present work, nickel-based powders were used to obtain thermally sprayed coatings with improved wear resistance. The feedstock materials chosen for the current study contained, besides the Ni matrix, different additions of elements like Cr and B, which are carbide-forming elements and consolidate the resistance of the resulting coatings against wear, as well as Fe, which contributes to the reduction of chromium solubility in the Ni phase, promoting the formation of hard precipitates [27,28]. For comparison, three types of powders with different chemical compositions and characteristics were applied to a tempered steel substrate using oxyacetylene flame spraying, and subsequently, the coatings were remelted by induction. One type of powder is commercially available, and the other two types were specially developed for the current study. The resulting coatings were characterized in terms of tribological properties, establishing a correlation between the intrinsic characteristics of the feedstock powder and the corresponding wear behavior of the coatings. A comparison between as-sprayed and inductively remelted coatings was also carried out.

2. Materials and Methods

NiCrBSi feedstock powders were considered in the current study to obtain the thermally sprayed coatings. For comparison, three types of powders with different chemical compositions were identified. The powders were manufactured by LSN Diffusion, Llandybie, United Kingdom, one type of powder being commercially available as LSN 330 (denoted in this study KS-IC-45), and the other two types being specially developed for the Karl Schumacher Company, Bochum, Germany. Powder composition and particle sizes provided by the manufacturer are presented in Table 1. The Karl Schumacher Company has given its consent for the processing of data. Generally, the elements Cr and B, which are present in the chemical composition of the powders, increase the wear resistance since they are carbide-forming elements [5]. Therefore, the newly developed powders (KS-IC-55S and KS-IC-55 respectively) contain higher amounts of Cr and B.

Table 1. Chemical composition of the nickel-based powders.

Trade Name	Ni [%]	Cr [%]	B [%]	Si [%]	Fe [%]	C [%]	Grain Size [μm]
KS-IC-45	Bal.	6.02	1.12	4.19	1.50	0.25	–106 + 45
KS-IC-55S	Bal.	10.10	2.49	3.51	4.00	0.40	–106 + 45
KS-IC-55	Bal.	13.02	2.80	4.19	5.12	0.42	–106 + 45

All the coatings were flame sprayed on the same substrate material, which was preheated at 120 °C to facilitate adhesion. The substrate consisted of a tempered steel 1.7227, with the nominal chemical composition presented in Table 2. Hardness measurements were performed on the substrate material using a Zwick Micro Hardness tester, ZwickRoell, Ulm, Germany. The applied load used for determining the Vickers microhardness was 3 N for 15 s. The results showed that the steel substrate had an average Vickers hardness of $315 \pm 10 \text{ HV}0.3$.

Table 2. Chemical composition of the substrate material.

Steel	C [%]	Si [%]	Mn [%]	P [%]	S [%]	Cr [%]	Mo [%]	Al [%]
1.7227	0.42	0.26	0.73	0.012	0.023	1.13	0.21	0.027

Prior to the thermal spraying, the substrate surface was subjected to a two-step cleaning process. In the first step, the parts were degreased with alcohol to remove moisture and the organic residues left after the turning process. In the second step, the surface was sandblasted with cast iron hard particles to remove the oxides and to obtain a rough surface profile that might enable better mechanical anchorage of the subsequently thermally sprayed particles. In the sandblasting process, the abrasive material was accelerated using compressed air towards the substrate at an angle of 60 degrees to avoid the impregnation of hard particles on the substrate's surface. During sandblasting, all the superficial impurities were removed and a roughness of $R_a = 75 \mu\text{m}$ was obtained. The roughness was evaluated with a contact profilometer, Mitutoyo SJ-201, Mitutoyo Europe GmbH, Neuss, Germany.

Thermal spraying was performed with a mixture of acetylene and oxygen gases (1:2) using a Metatherm 5P gun, Metatherm Verschleißschutz GmbH, Bexbach, Germany, with a total gas flow of 38.7 L min^{-1} and a spraying distance of 200 mm at a linear speed of 6.5 mm s^{-1} . The coatings consisted of several layers, up to a final thickness of approx. 1.2 mm for all three types of powders.

The as-sprayed coatings were post-processed by electromagnetic induction heating using an EKOHEAT 200/30 heating instrument, Ambrell, The Netherlands, working in the 15 kHz to 40 kHz frequency range. The remelting process consisted firstly of a preheating step at a lower power and faster velocity than applied for the remelting process itself. The induction remelting process optimization was reported in previously published work [29].

Preceding the deposition step, to characterize and compare the three types of feedstock powders, a scanning electron microscope (SEM), Philips XL30 ESEM, Eindhoven, The Netherlands, equipped with an energy-dispersive X-ray spectrometer (EDX), Ametek, PA, USA, and a confocal laser scanning microscope (CLSM), VK-X 3D, Keyence, Mechelen, Belgium, was used for microstructural and chemical analyses, while X-ray diffraction (XRD), Philips X'Pert MDP X-ray diffractometer, Malvern PANalytical, Malvern, UK, was used to identify the chemical phase composition. The XRD measurements were performed in the $20\text{--}100^\circ$ 2θ range at a working voltage of 45 kV and a current of 40 mA, with a 2θ scanning step of 0.015° . The same equipment was used to characterize the as-sprayed and induction-remelted NiCrBSi coatings. The cross-section of the powders and of the resulting coatings was obtained by conventional metallographic preparation according to the ASTM E1920-03 [30], comprising cold mounting in epoxy resin; grinding with 180, 320, and 800 grit SiC abrasive paper; and rough polishing with diamond suspension ($3 \mu\text{m}$ and $6 \mu\text{m}$).

Sliding wear was chosen to investigate the tribological properties of the as-sprayed and induction-remelted coatings using a ball-on-disk arrangement according to the ASTM G99-17 standard [31]. The measurements were accomplished with the aid of a CSM Instruments Tribometer, Peseux, Switzerland, on the ground surface of the samples under dry sliding conditions at ambient temperature and 50% humidity, with a normal load of 10 N, linear speed of 15 cm s^{-1} , and a total sliding distance of 566 m and 943 m for the as-sprayed and induction-remelted coatings, respectively. The counterpart selected for the tests was a WC-Co ball of 6 mm diameter. The testing parameters were selected to simulate the aggressive wear conditions that may occur in normal industrial operation. During testing, the variation in the coefficient of friction (COF) with the distance was automatically recorded. For each type of powder, three measurements in identical conditions were performed. The wear track profiles were evaluated using CLSM micrographs and the wear rate was estimated according to the Archard equation [32].

3. Results and Discussion

3.1. Powder Morphology and Properties

The particle morphology and size distribution of NiCrBSi feedstock powders are illustrated in Figure 1. As observed, for each type of powder, the particle dimensions are in the same range as the values given by the manufacturer. The KS-IC-55S powder has a less uniform particle size distribution, which may lead to a much more porous coating as well as unmelted particles occurrence during the flame-spraying process compared to that of the

powders with equal size dimensions since the larger particles need more time to reach a fully molten state [33]. At the same time, the powder with smaller dimensions, which is heated much faster than the powder with larger particles, generates more oxides in the resulting as-sprayed coatings.

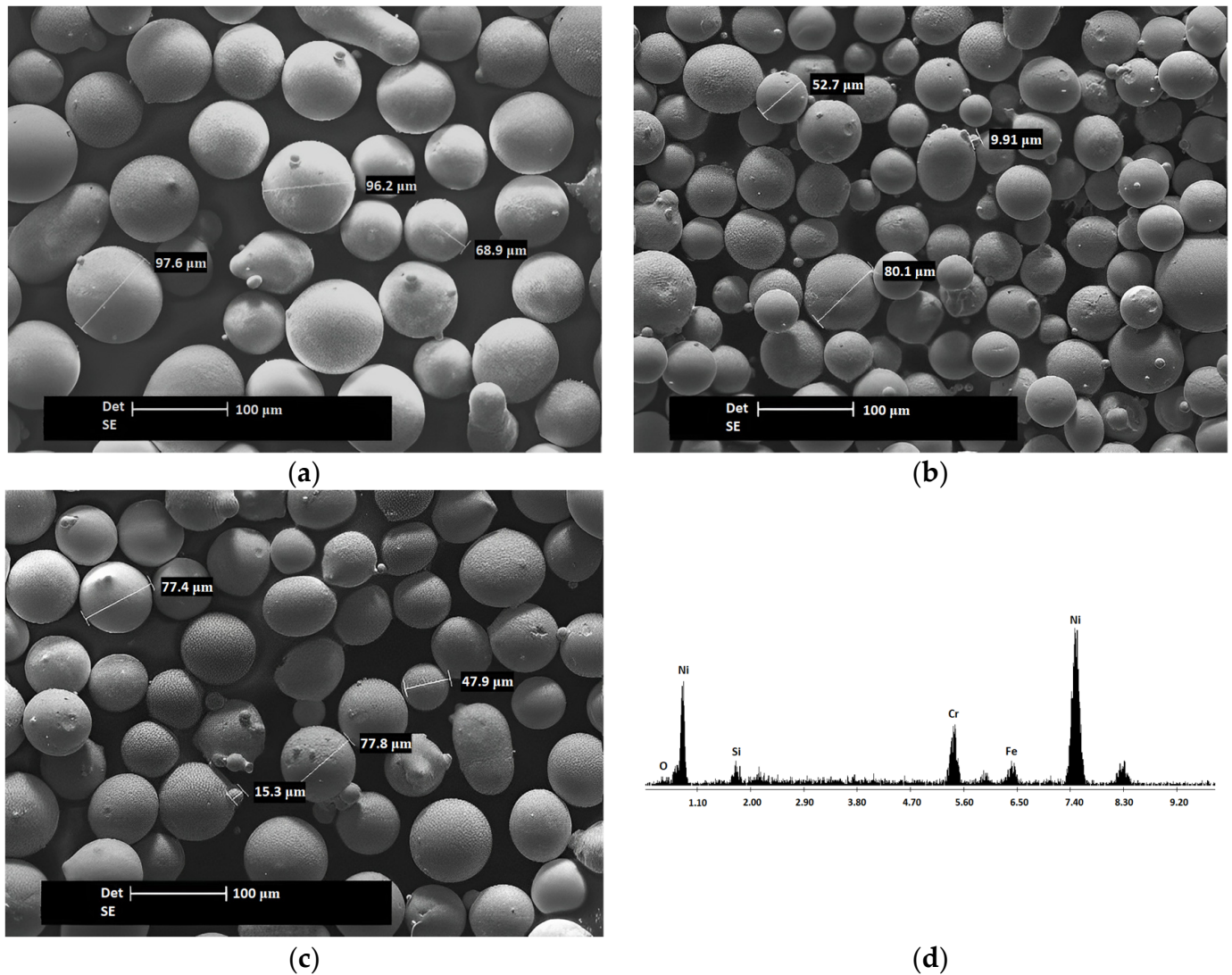


Figure 1. SEM micrographs of the NiCrBSi powders: (a) KS-IC-45; (b) KS-IC-55S; (c) KS-IC-55; (d) EDX spectrum of the NiCrBSi powders.

All three types of powders are obtained by a gas atomization process with water collection; consequently, a completely spherical shape is observed with similar chemical composition, as presented in Figure 1d. This synthesis method has a high production efficiency, and the obtained powder combines the properties of gas and water atomization technology. The particle surface is smooth and some particles present minor satellites attached to the surface. Furthermore, the spherical shape assures the free flow of the powder, which is a critical condition for the industrial production of thermally coated parts by flame spraying. A good flowability increases productivity by facilitating a more regular feed rate [34], and at the same time, it increases consistency in the obtained coatings. To characterize the powders' flowability and apparent density, the Hall flowmeter method is used, according to the international standard ISO 4490:2008 [35]. In this method, a weighed mass (50.0 g) of unlubricated powder is timed as it flows through the calibrated orifice of a flowmeter funnel to determine the flow rate [24]. The mass of powder per

unit volume is simultaneously recorded and reported as apparent density [36]. The ability of a powder to flow is a function of interparticle friction, correlated with the particle size distribution. Generally, larger particles tend to flow more easily than the smaller ones, which are considered cohesive ($d_p < 100 \mu\text{m}$) [37]. Table 3 presents the results of the analyses, considering both the flow properties and their apparent densities. A better flowability was determined for the KS-IC-45 powder, which presents a narrower particle size distribution with a higher fraction of large particles, while in the case of KS-IC-55S powder, where less uniform particle size distribution was observed, the flow rate and the apparent density were significantly reduced.

Table 3. Physical tests of NiCrBSi powder.

Powder Type	Apparent Density [g cm^{-3}]	Hall Cup Flow [$\text{s } 50^{-1} \text{g}^{-1}$]
KS-IC-45	4.70 ± 0.05	15.3
KS-IC-55S	4.40 ± 0.02	14.1
KS-IC-55	4.70 ± 0.03	15.1

A broader size distribution of the powder leads to different particle momentums during deposition and thus distinct particle trajectories and velocities correlated with dissimilar temperature distributions upon impact with the substrate [34].

For a more detailed characterization, the powders were analyzed in cross-section to observe their inner structure. Figure 2 shows the NiCrBSi feedstock powders in cross-section, with the particles presenting a uniform chemical composition but with large gaps in the center (internal porosity) for all three types of powders. These gaps are generally undesired since they lead to overheating of the particles during the spraying process, promoting more intense oxidation and delivering a coating with two types of porosity, an interconnected one (interlamellar porosity) resulting from the layer-by-layer coating formation, and a closed one that may arise from the internal porosity of the particles [38]. Due to this fact, a subsequent heat treatment is in this case strongly recommended; this brings the coating to a semi-molten state, eliminating not only the voids obtained during the deposition process but also the internal pores attained from the particles' structure.

3.2. Phase Composition of the Powders

Figure 3 shows the diffraction patterns of the three NiCrBSi feedstock powders, revealing their main initial phase compositions. The complexity of the NiCrBSi system enables the formation of different phases according to the elements' ratios in the chemical composition of the powder. All the investigated powders present a high level of crystallinity, described by the occurrence of well-defined peaks. The KS-IC-45 powder, having around 6 wt.% Cr and a higher Ni content, consists mainly of 70% Ni (cubic), 14% NiSi (orthorhombic), and 11% Ni₃B (orthorhombic). The KS-IC-55S powder, with a greater Cr content (10 wt.%), presents in the structure only 48% Ni; besides this, there is a 36% ternary Cr₃Ni₅Si₂ transition metal silicide phase crystallized in the cubic system that arises due to the increased chromium content. This specific phase is beneficial for the tribological behavior since it has been frequently reported to perform excellently under dry sliding test conditions [39] due to its intrinsic high hardness and strong covalent bonds [40]. Additionally, a 5% CrNi phase is detected, crystallized in the cubic system, and a greater content of hard polycrystalline orthorhombic boride CrB than that in the previously discussed powder is observed. The third powder, KS-IC-55 (containing 13 wt.% Cr) indicates similar phases to KS-IC-55S, but with a different percent distribution, including a smaller amount of ternary Cr₃Ni₅Si₂ and an additional 13% intermetallic NiFe phase formed due to the slightly higher Fe content in the powder.

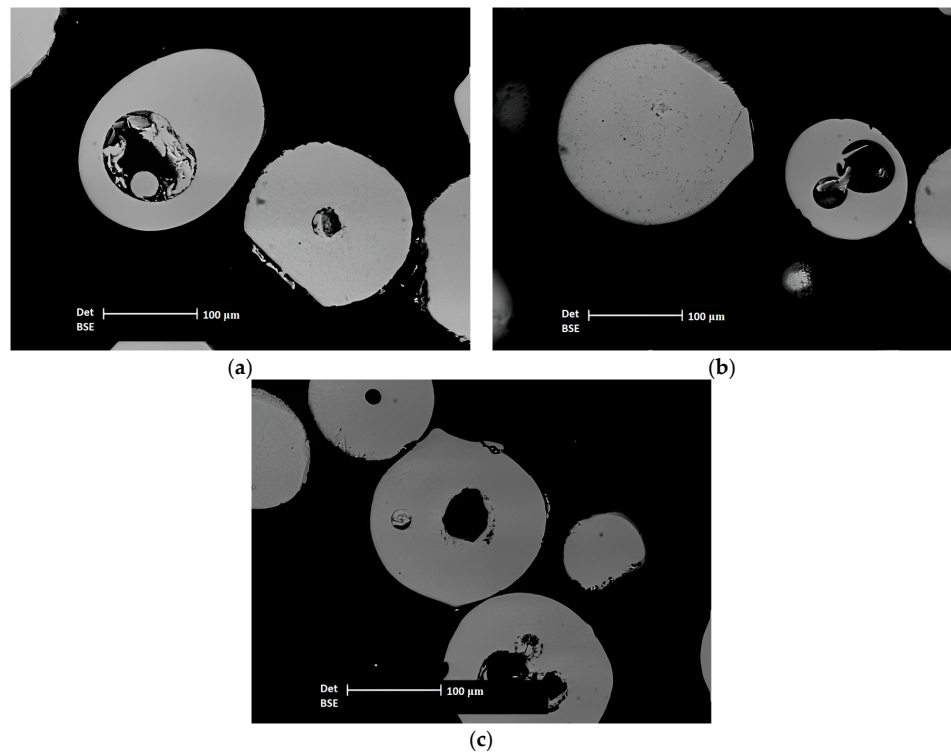


Figure 2. SEM cross-section micrographs of the NiCrBSi powders: (a) KS-IC-45; (b) KS-IC-55S; (c) KS-IC-55.

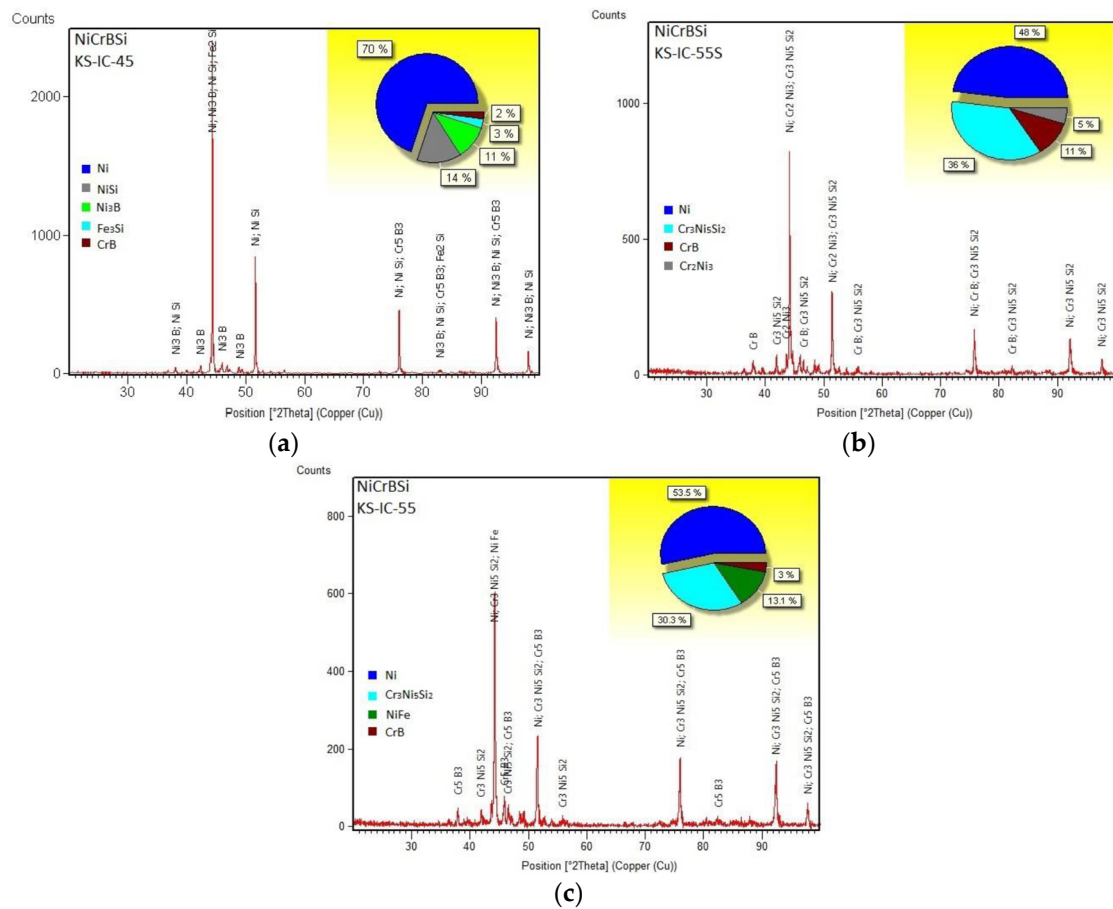


Figure 3. XRD diffraction patterns of the NiCrBSi powders: (a) KS-IC-45; (b) KS-IC-55S; (c) KS-IC-55.

3.3. Morphology of the As-Sprayed Coatings

All three types of powders generate similar coating structures in cross-section, each containing varying levels of defects, as a result of the identical working conditions applied during the flame-spraying process with oxyacetylene. In the as-sprayed condition (Figure 4a), the coating's homogeneity is relatively low; however, no cracks are detected. The coatings exhibit poor adhesion to the substrate due to the excessive porosity and the presence of unmelted particles and inclusions along the interface, typical for flame-sprayed coatings, as illustrated in Figure 4b. Moreover, unmelted particles, unbounded splats, and pores (highlighted in Figure 4d), more concentrated on the upper side of the coating, can be observed; such defects affect the bond strength due to the low particle cohesion [38]. The pores generated by entrapping gas bubbles are mostly spherical, while those produced by other mechanisms have different irregular shapes, some of them following the contour of the unmelted particles. The porosity degree was estimated separately for each specimen using SEM micrographs acquired at a $1000\times$ magnification in three different regions of the cross-sectioned sample, with analysis conducted in ImageJ software (a free open-source Java-based program, v.1.54d) according to the ASTM E2109-01 standard [41]. The average porosity values are comparable for all three types of coatings in the as-sprayed state, ranging between 12 and 14% and presented along with the standard deviation in Figure 5. The slightly smaller porosity values obtained for the KS-IC-45 coatings may be correlated with the better flowability and the narrower particle size distribution observed in the analysis of the feedstock powder.

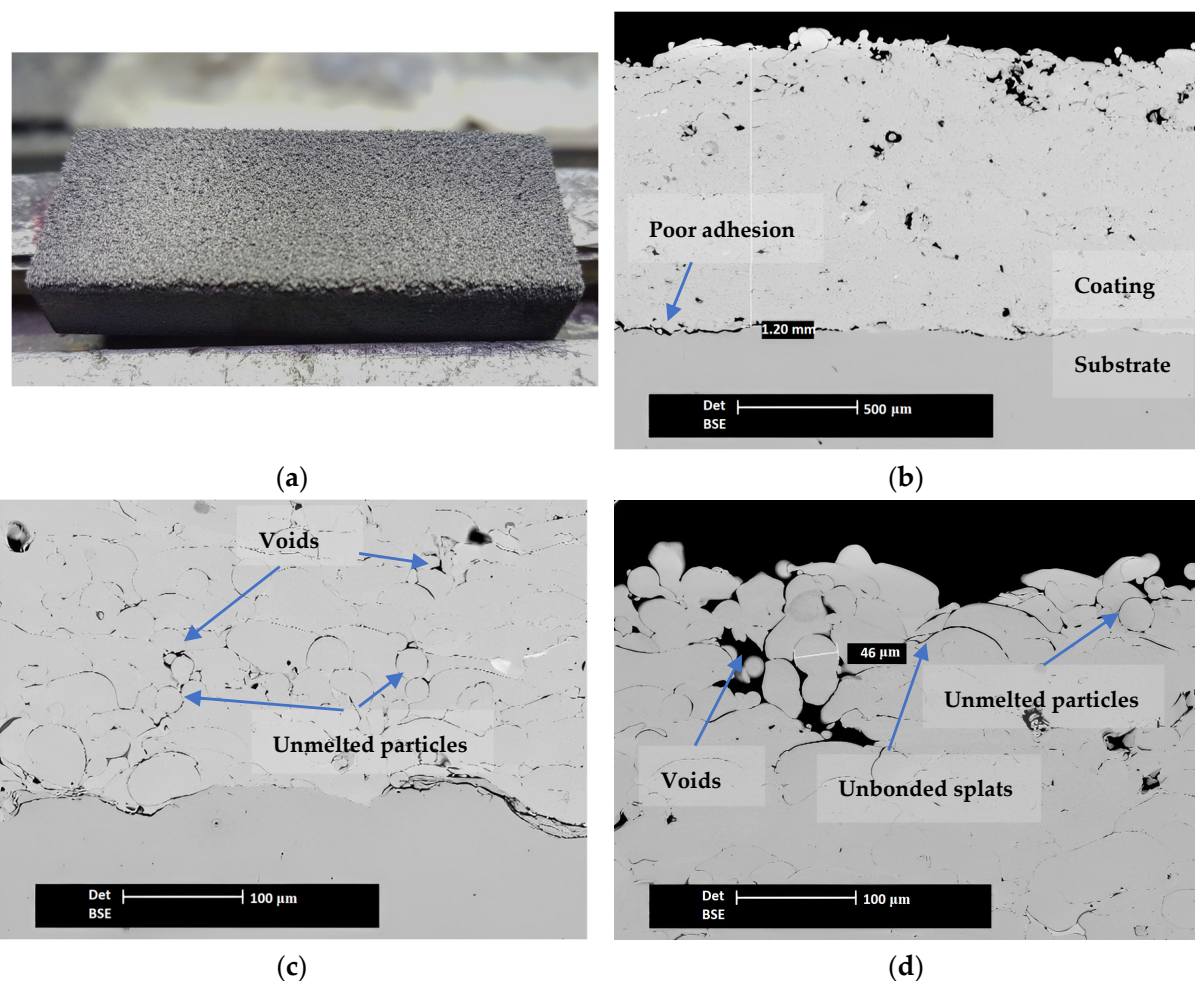


Figure 4. (a) View of the KS-IC-45 as-sprayed coating, SEM cross-section micrograph of the as-sprayed KS-IC-45 powder (b) whole thickness; (c) magnified interface region; (d) magnified surface region.

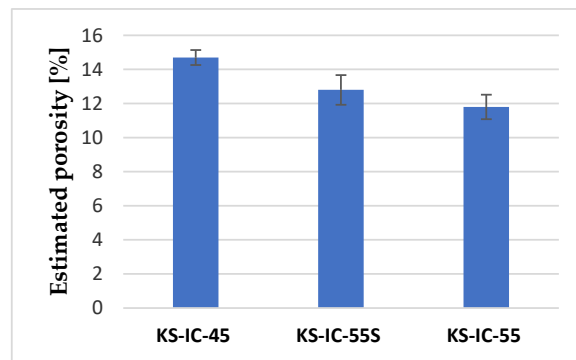


Figure 5. Average porosity of the as-sprayed coatings estimated using ImageJ software.

3.4. Tribological Behavior of the As-Sprayed Coatings

Following the oxyacetylene flame-deposition process, the coatings were investigated regarding their tribological behavior. Sliding wear was chosen to investigate the as-sprayed coatings using a ball-on-disk arrangement. Before the sliding wear tests, the samples in the form of rectangular coupons were ground with abrasive SiC paper (180 grit size) to flatten the rough surface obtained during flame spraying to a roughness of $R_a = 0.8 \mu\text{m}$ and then cleaned with acetone and dried in air.

As can be seen in the COF evolution plotted against distance and time, as presented in Figures 6–8, the superficial layer of the deposited coatings does not have a very good bond or stability since it presents only mechanical adhesion by clamping to the previously deposited layer. This leads to a very unpredictable friction behavior; in all cases, the COF is not stable during the measurement and presents a quite large deviation from the average value. The non-uniform wear track profile observed in the corresponding CLSM micrographs may be attributed to the low intersplat cohesion, which caused the facile pull-out of material. In the case of KS-IC-45 powder (Figure 6), it can be remarked that since it has a lower Cr content and reduced hardness due to a higher ductile Ni phase amount, after the first 226 m of the sliding testing, the COF stabilized because the softer asperities were more easily flattened by the hard WC-Co ball. In this situation, the COF values ranged from 0.5 to 0.86, with the maximum values being reached in the transitional phase, where some of the pulled-out particles were temporarily locked between the sliding surfaces. For the other two types of powders, a less stable friction coefficient was observed, and for the KS-IC-55S, a much finer wear track was measured (Figure 7), which may be due to the finer granulation of the powder compared to that of KS-IC-55 (Figure 8). In both cases, slightly smaller maximum COF values were observed, since the feedstock powders consist of harder Cr- and B-containing phases.

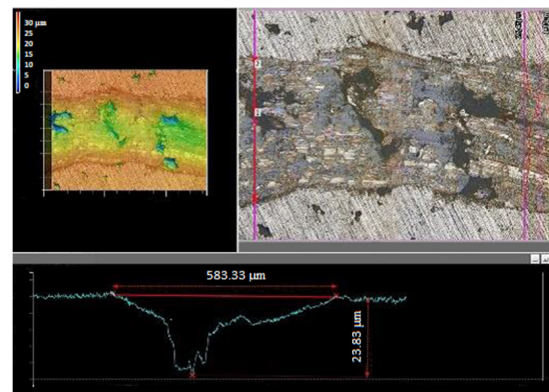
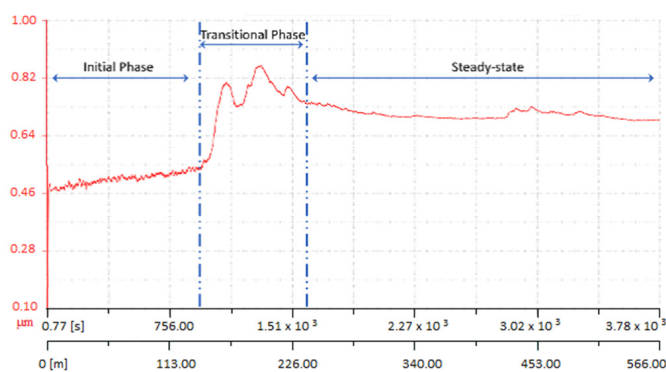


Figure 6. Friction coefficient evolution and wear track of as-sprayed KS-IC-45 coating.

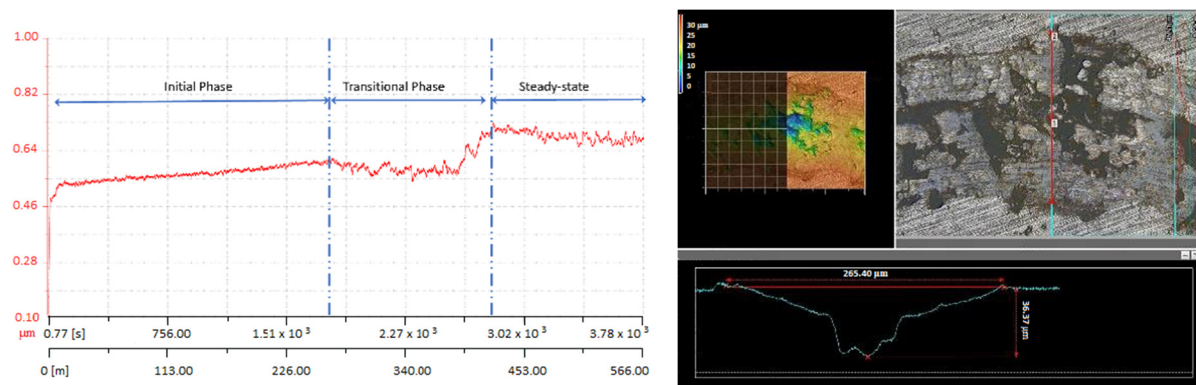


Figure 7. Friction coefficient evolution and wear track of as-sprayed KS-IC-55S coating.

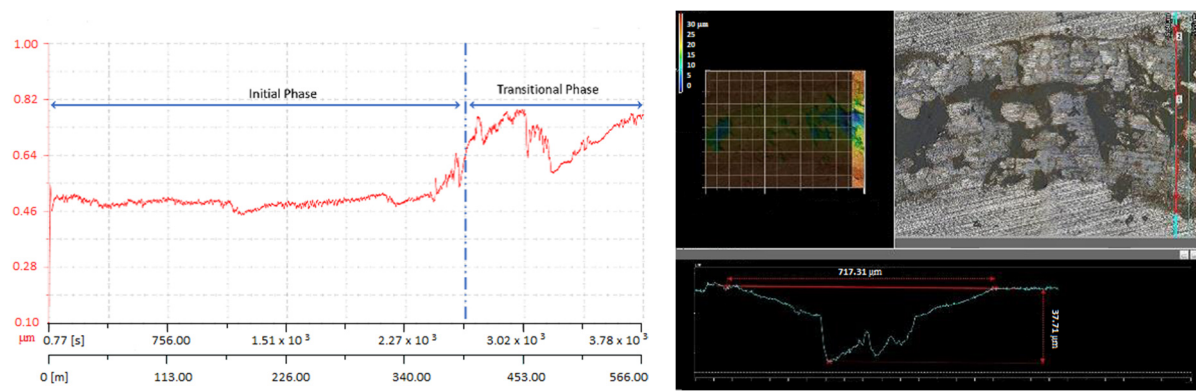


Figure 8. Friction coefficient evolution and wear track of as-sprayed KS-IC-55 coating.

Regarding the wear tracks, it can be observed that the hard particles were dragged from the coatings during the sliding tests and microgrooves appeared, while the friction coefficient was very unstable. This reveals that the main wear mechanisms were abrasive and correlated with intense wear losses due to the poor intersplat cohesion typical of flame-sprayed coatings [10]. Furthermore, it is also observed that, depending on the chemical composition, once the Cr content increases the initial phase is extended and the COF remains at low values. For all three types of coatings, a transitional zone was observed that presents an anomaly in the case of KS-IC-45 powder, where the coefficient of friction jumps in this region to an approximately double value for a short period, and at the exit of the transitional zone, it stabilizes at an intermediate value, entering the steady state until the end of the measurement. Contrarily, in the case of KS-IC-55 powder, the steady-state zone did not appear in the measured range, and the test ended in the transition zone. The most stable COF with the lowest standard deviation was observed for the KS-IC-55S powder, which may be attributed to the increased content of the $\text{Cr}_3\text{Ni}_5\text{Si}_2$ metal silicide phase.

3.5. Morphology of the Induction-Remelted Coatings

The CLSM micrographs presented in Figure 9 display the uniform microstructure of the NiCrBSi coatings after the induction remelting process. In all three cases, the initial boundaries between the particles observed in the as-sprayed condition were eliminated due to the self-fluxing character of the NiCrBSi alloy. The unmelted particles were totally fused through the remelting process and the oxides formed during flame spraying were reduced due to the presence of B and Si [38]. In the remelting process, a low melting point eutectic may be formed, and therefore, the porosity of the coatings was consistently reduced from about 12–14% for the as-sprayed coatings to 0.5% in the case of KS-IC-45, 0.9% in the case of KS-IC-55, and 1.1% for the KS-IC-55S powder, as presented in Figure 10. The greatest reduction in porosity obtained for the KS-IC-45 powder may be attributed to the lower Cr

content, which in this case has a positive effect. The minor difference in porosity values between the KS-IC-55S and KS-IC-55 can be explained by the fact that the latter has a higher content of elements that favor the self-fluxing process, namely Si and B.

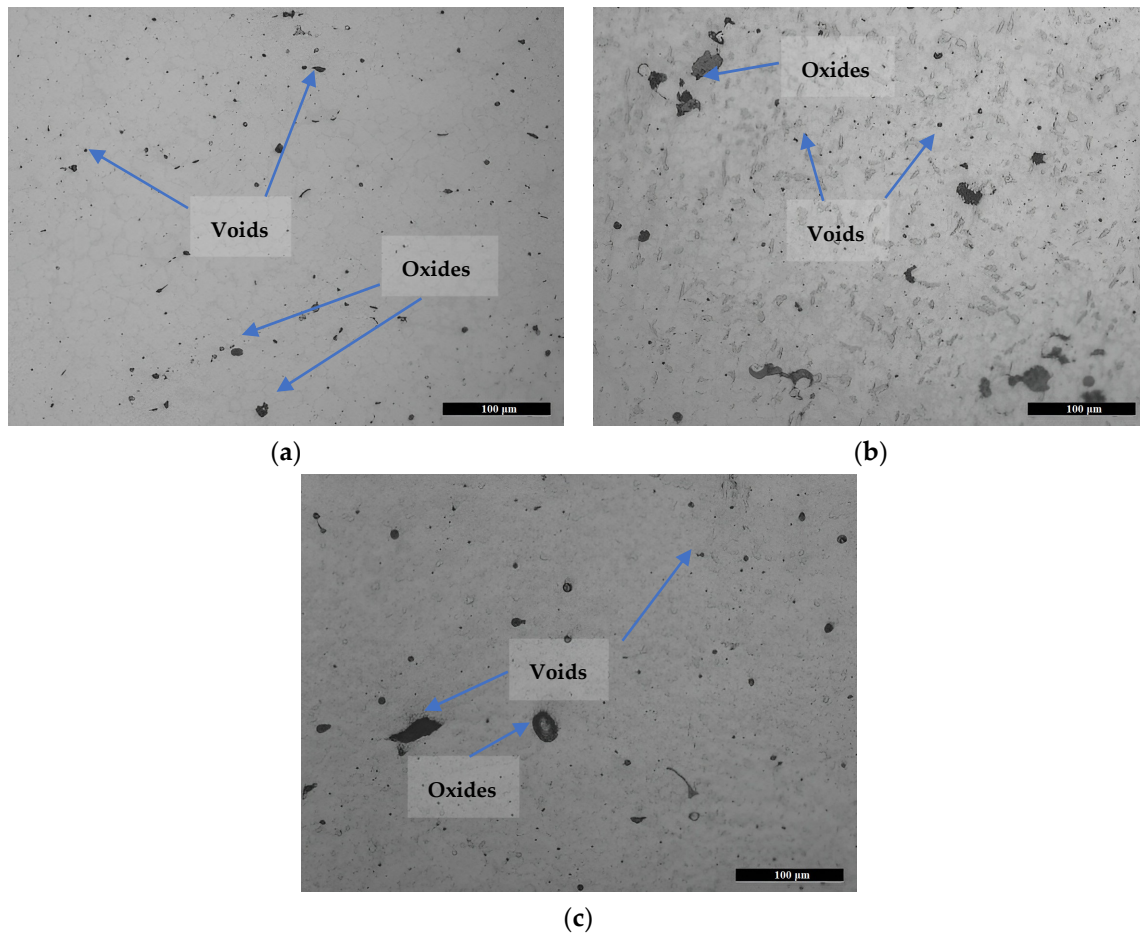


Figure 9. CLSM cross-section micrographs of the induction-remelted (a) KS-IC-45; (b) KS-IC-55S; (c) KS-IC-55 powder.

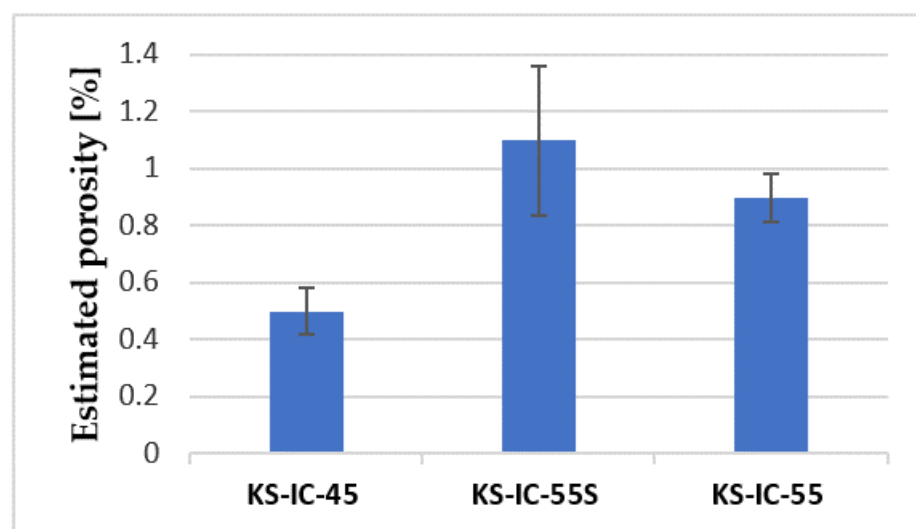


Figure 10. Average porosity of the induction-remelted coatings estimated using ImageJ software.

Compared with the results of other studies on the same type of NiCrBSi powders but employing other deposition and remelting processes, a similar reduction of porosity was observed in this study. Bergant et al. remelted NiCrBSi as-sprayed coatings in a furnace with a protective argon atmosphere and managed to obtain a percentage of 0.83% porosity [16], while Karimi et al. succeeded in obtaining a minimum porosity of 1.9% by remelting the coatings with an oxyacetylene flame using a torch [38].

The CLSM cross-section micrographs presented in Figure 11 show the whole-thickness structure of the induction-remelted coatings, where in all cases, the porosity was significantly reduced and the intersplat boundaries disappeared. The densification achieved during the remelting process led to a slight reduction of the coatings' thicknesses compared to those in the as-sprayed state. The remelting process resolved the initial particle boundaries observed on the as-sprayed coatings due to the fluxing character of the NiCrBSi alloy [38]. The enhanced cohesion between splats and the denser and more uniform microstructure has also a positive impact on the wear behavior of the remelted coatings. Moreover, better metallurgical bonding between the coating and substrate was achieved.

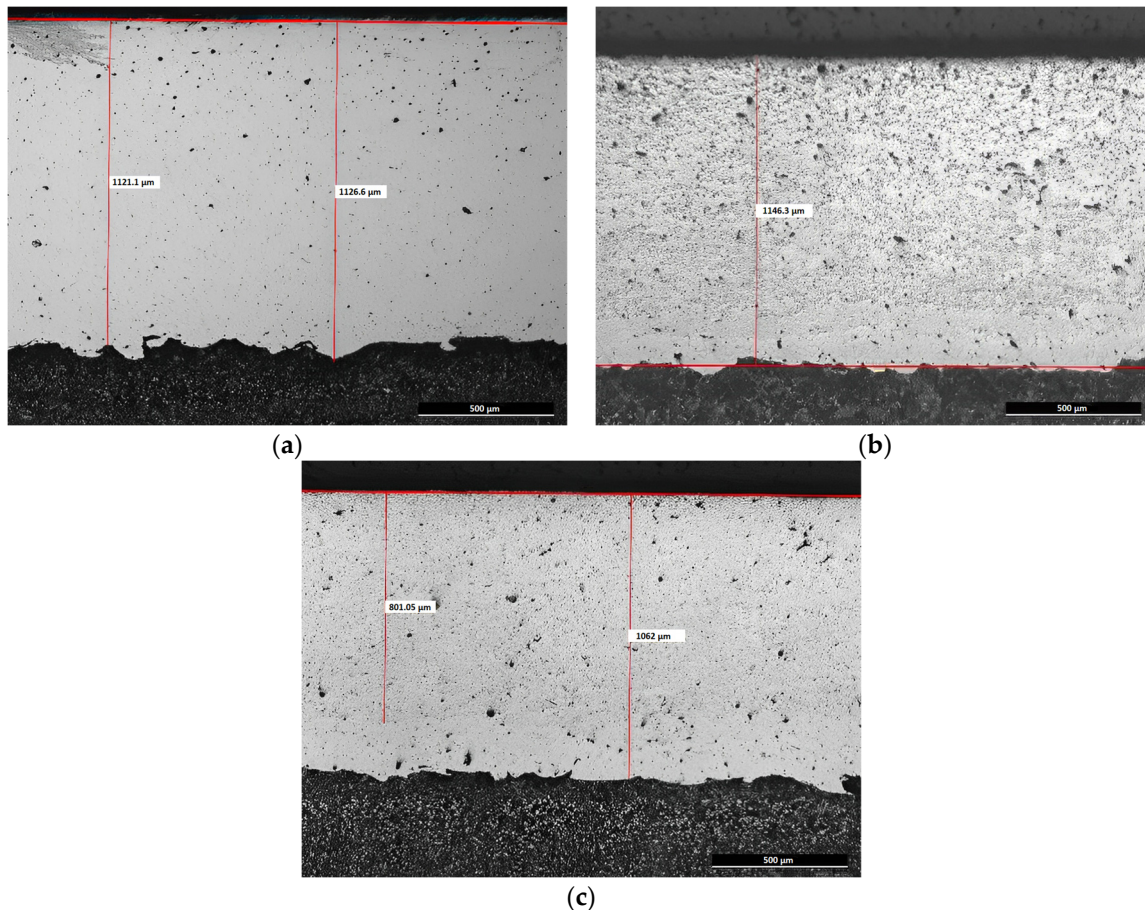


Figure 11. CLSM cross-section micrographs of the whole-thickness induction-remelted (a) KS-IC-45; (b) KS-IC-55S; (c) KS-IC-55 powder.

3.6. Phase Composition of the Induction-Remelted Coatings

According to the XRD diffraction patterns (Figure 12) recorded for the inductively remelted coatings, the nickel matrix is predominant in all three types of powders and remains the same for the correspondent coatings. After the heat treatment, the nickel-free phase content was slightly reduced compared to that in the feedstock powder, and a more homogeneous phase composition for all three types of coatings was created, all of them having the same four significant phases in different ratios. The presence of intermetallic Ni₃B and CrB confirms the efficiency of the remelting process, which generated sufficient

temperature and time for B atoms to diffuse and combine with the Ni and Cr elements. Moreover, the formation of borides may potentially influence the wear behavior of the coatings, as already reported by other studies [9]. The presence of silicides in the form of the $\text{Cr}_6\text{Ni}_{16}\text{Si}_7$ phase in all three types of coatings increases the stability at high temperatures; at the same time this phase clearly improves the wear behavior.

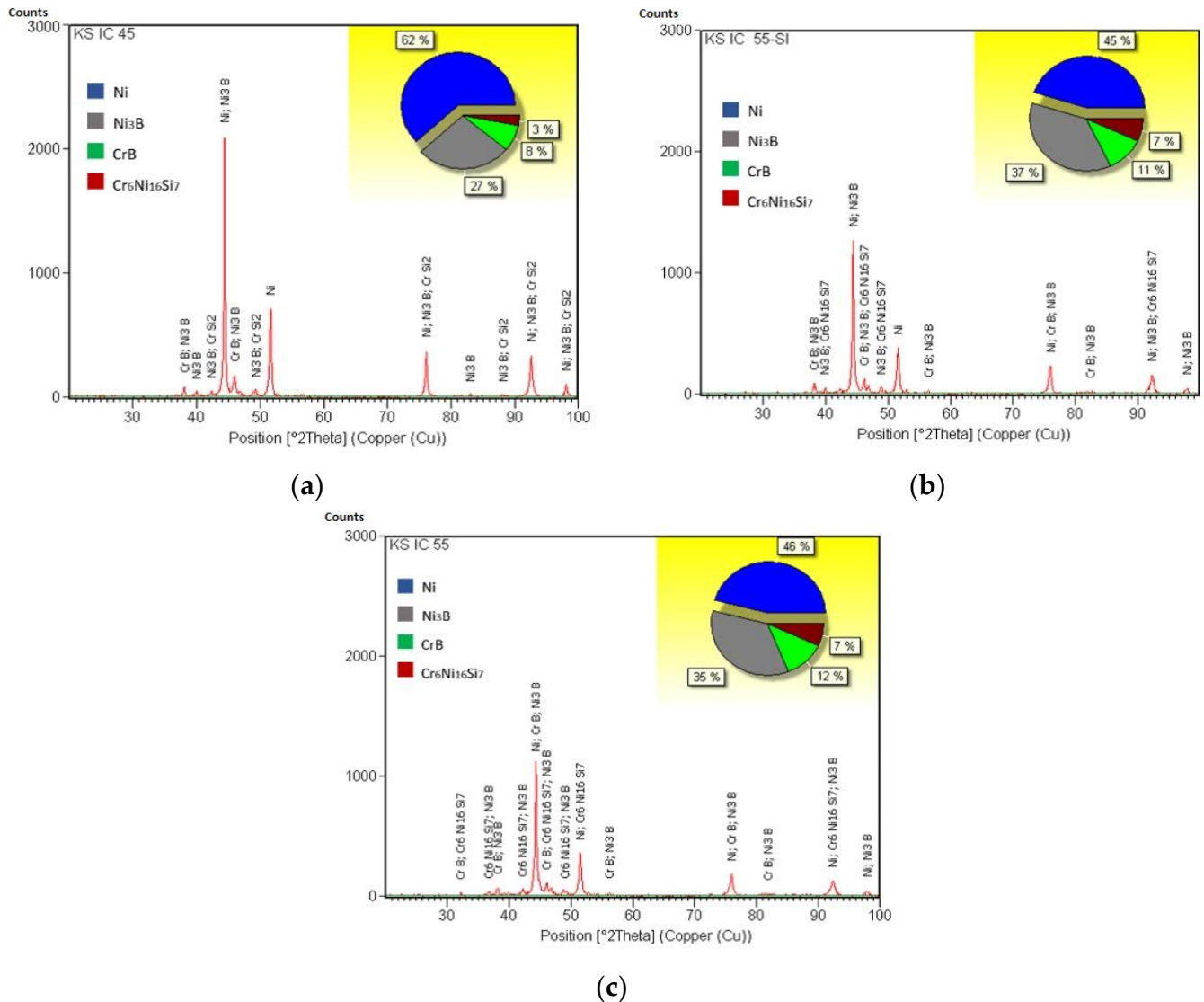


Figure 12. XRD diffraction patterns of the NiCrBSi inductively remelted coatings: (a) KS-IC-45; (b) KS-IC-55S; (c) KS-IC-55.

3.7. Tribological Behavior of the Inductively Remelted Coatings

Sliding wear testing of the inductively remelted coatings was performed under identical working conditions as for the as-sprayed coatings but for a longer total distance of 942 m. The friction coefficient evolution and the wear tracks acquired with the CLSM are presented in Figures 13–15. Generally, the mean friction coefficient measured for the induction-remelted coatings was similar to that of the as-sprayed coatings; the main differences consisted in the variation degree of the values during the tests and in the aspect of the worn surfaces after the tests. While in the case of as-sprayed coatings, the COF importantly fluctuated, the inductively remelted coatings presented great stability, and the COF reached a steady state after only 150 m of sliding distance. Moreover, the remelted samples showed no transitional phase and the COF directly passed from the incipient phase to the steady

state, an aspect which can be explained based on the superior density of the remelted coatings. The beneficial effect of the remelting process is reflected in the COF evolution and wear rates and is primarily assigned to the mitigation of defects such as pores and poor splat bonding, correlated with a better homogeneity of the coatings [13]. KS-IC-45 powder generated a slightly higher friction coefficient among the remelted coatings than the other two powders, and this can be attributed to the lower hardness values due to the greater content of the ductile Ni phase (62%). The hardness of the remelted coatings proportionally increased with the Cr content as well as with the total content of borides and silicides in the phase composition of the coating, having a direct influence on the abrasive wear resistance [13]. Similar studies on NiCrBSi remelted coatings have shown that an increase in Cr content provides a decrease in the wear rate [26].

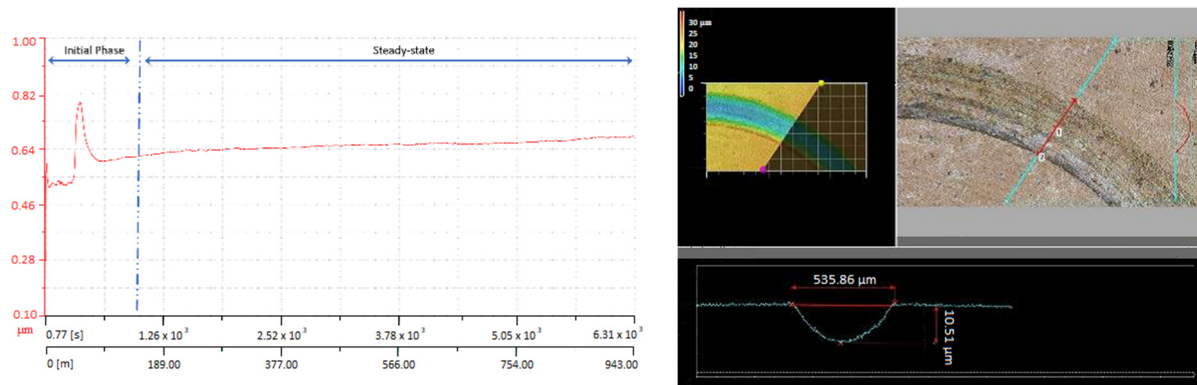


Figure 13. Friction coefficient evolution and wear track of inductively remelted KS-IC-45 coating.

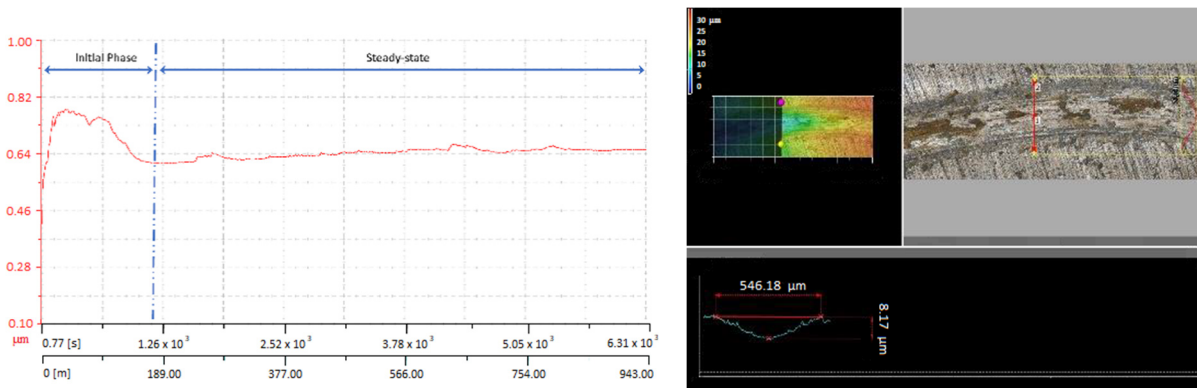


Figure 14. Friction coefficient evolution and wear track of inductively remelted KS-IC-55S coating.

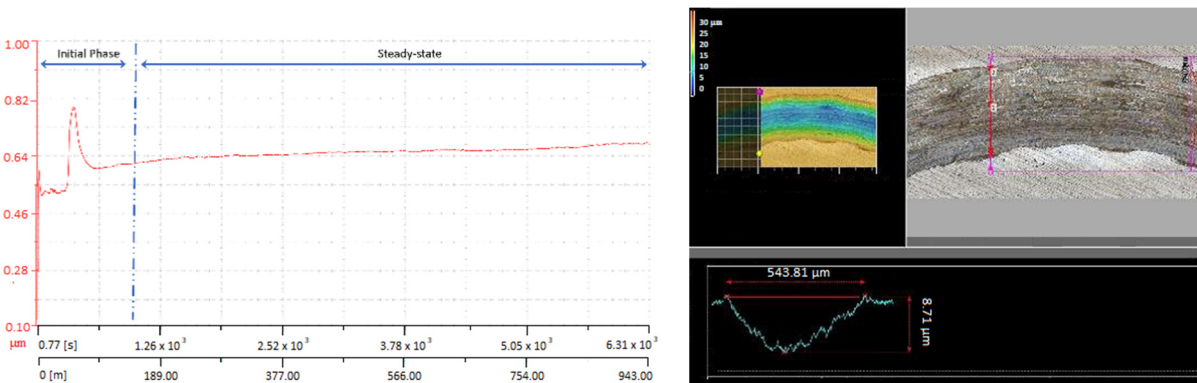


Figure 15. Friction coefficient evolution and wear track of inductively remelted KS-IC-55 coating.

Furthermore, from the analyzed wear track segment, a semi-round worn section with a smaller width than that of the as-sprayed coatings was observed, which may be attributed to the lower degree of penetration of the counterpart in the material, resulting in a less pronounced wear rate for both partners. The best-performing remelted coating in terms of wear was the IC-KS-55S. The areas of the worn track cross-section and worn cap diameter, as determined by microscopic measurements, were used to calculate the specific wear of the inductively remelted coatings according to the Archard equation [32]. The bar chart presented in Figure 16 displays the average wear rates of the inductively remelted coatings and their standard deviation. The calculated values are in good agreement with similar NiCrBSi coatings reported in the literature [8].

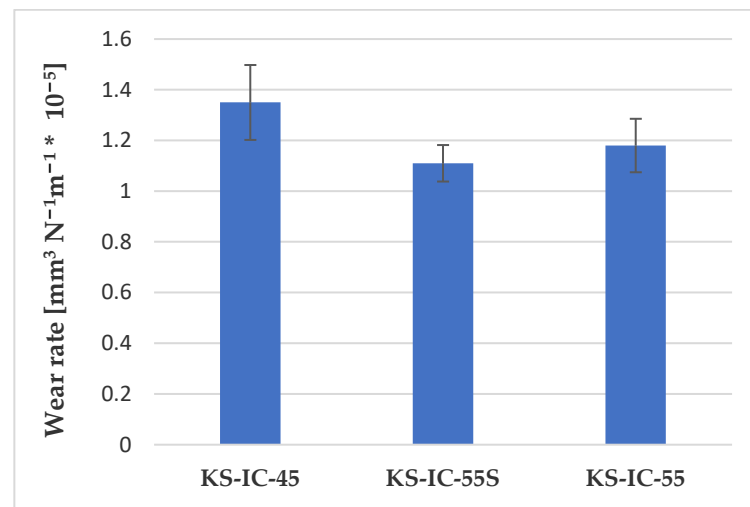


Figure 16. Wear rates of the inductively remelted coatings.

4. Conclusions

Three types of NiCrBSi powders with different chemical compositions and characteristics were applied to a tempered steel substrate using oxyacetylene flame spraying. The morphology, chemical composition, flowability, and apparent density of the feedstock powders were investigated and correlated with the wear resistance of the as-sprayed and induction-remelted coatings. All powders presented a uniform chemical composition but also internal porosity, which led to more intense oxidation, thus delivering a structure with several defects in the case of the as-sprayed coatings. Consequently, an induction remelting process was applied, which led to the following findings:

- In the case of the remelted samples, the porosity was significantly reduced and the intersplat boundaries disappeared due to the fluxing character of the NiCrBSi alloy.
- Moreover, during the remelting treatment, a more homogeneous phase composition for all three types of coatings was created and more wear-resistant phases, like intermetallic Ni₃B and CrB, were generated.
- In the case of as-sprayed coatings, a more unstable friction coefficient was observed, associated with an abrasive wear mechanism and promoted by the poor intersplat cohesion and the higher porosity. During the sliding wear tests, the hard particles were dragged out from the coatings and microgrooves appeared, while the COF evolution consisted of three main phases. The steady state was achieved only after 226 m of sliding distance in the case of KS-IC-45 and later for the other two powders, and the most stable COF was observed for the KS-IC-55S coating.
- The varying degree of COF values during the sliding tests and the aspect of the worn surfaces were significantly improved after the remelting process. This positive effect is primarily attributed to the mitigation of defects, such as pores and poor splat bonding, and the increased homogeneity of the coatings.

- The hardness and the wear resistance of the remelted coatings proportionally improved with the increase in Cr content in the feedstock powder, as well as with the total content of borides and silicides in the phase composition of the coating, having a direct influence on the abrasive wear resistance. The best-performing remelted coating in terms of wear was the IC-KS-55S, having the lowest wear rate and the narrowest COF fluctuation.

Author Contributions: Conceptualization, G.M. and V.A.S.; methodology, P.-C.V. and N.K.; validation, P.-C.V. and N.K.; investigation, R.M., P.-C.V. and N.K.; resources, G.M. and V.A.S.; data curation, R.M. and P.-C.V.; writing—original draft preparation, R.M. and P.-C.V.; writing—review and editing, R.M., I.-D.U., G.M. and V.A.S.; supervision, G.M. and V.A.S. All authors have read and agreed to the published version of the manuscript.

Funding: This research received no external funding.

Data Availability Statement: Not applicable.

Acknowledgments: We kindly appreciate the support of the company Karl Schumacher GmbH, Bochum, Germany, for the sample manufacturing.

Conflicts of Interest: The authors declare no conflict of interest.

References

1. Bolelli, G. Replacement of hard chromium plating by thermal spraying—Problems, solutions, and possible future approaches. *Surf. Eng.* **2009**, *25*, 263–269. [[CrossRef](#)]
2. Davis, J.R. *Handbook of Thermal Spraying*; ASM International: Novelty, OH, USA, 2004.
3. Harsha, S.; Dwivedi, D.; Agarwal, A. Influence of CrC addition in Ni-Cr-Si-B flame sprayed coatings on microstructure, microhardness and wear behavior. *Int. J. Adv. Manuf. Technol.* **2008**, *38*, 93–101. [[CrossRef](#)]
4. Ciubotariu, C.-R.; Frunzaverde, D.; Marginean, G. Investigations of Cavitation Erosion and Corrosion Behavior of Flame-Sprayed NiCrBSi/WC-12Co Composite Coatings. *Materials* **2022**, *15*, 2943. [[CrossRef](#)] [[PubMed](#)]
5. Aliabadi, M.; Khodabakhshi, F.; Soltani, R.; Gerlich, A. Modification of flame-sprayed NiCrBSi alloy wear-resistant coating by friction stir processing and furnace re-melting treatments. *Surf. Coat. Technol.* **2023**, *445*, 129236. [[CrossRef](#)]
6. Usana-ampaipong, T.; Dumkum, C.; Tuchinda, K.; Tangwarodomnukun, V.; Teeraprawatekul, B.; Qi, H. Surface and Subsurface Characteristics of NiCrBSi Coating with Different WC Amount Prepared by Flame Spray Method. *J. Therm. Spray Technol.* **2019**, *28*, 580–590. [[CrossRef](#)]
7. Okamoto, H.; Schlesinger, M.E.; Mueller, E.M. *Alloy Phase Diagram*; ASM International: Novelty, OH, USA, 2016; Volume 3.
8. Bergant, Z.; Batic, B.; Felde, I.; Sturm, R.; Sedlacek, M. Tribological Properties of Solid Solution Strengthened Laser Cladded NiCrBSi/WC-12Co Metal Matrix Composite Coatings. *Materials* **2022**, *15*, 342. [[CrossRef](#)] [[PubMed](#)]
9. Habib, K.; Cano, D.; Alvaro, J.; Serrano-Mira, J.; Llopis, R.; Moreno, D.L.; Mohammed, S.S. Effects of thermal spraying technique on the remelting behavior of NiCrBSi coatings. *Surf. Coat. Technol.* **2022**, *444*, 128669. [[CrossRef](#)]
10. Houdkova, S.; Smazalova, E.; Vostrak, M.; Shubert, J. Properties of NiCrBSi coating, as-sprayed and remelted by different technologies. *Surf. Coat. Technol.* **2014**, *253*, 14–26. [[CrossRef](#)]
11. Tabatabaei, F.; Ghasemi, B.; Mirzaee, O.; Adabifiroozjaei, E. The effect of WC-CoCr content on hardness and tribological properties of NiCrBSi coatings fabricated by the HVOF process. *Surf. Coat. Technol.* **2023**, *466*, 129506. [[CrossRef](#)]
12. Zhou, J.; Gou, W.; He, S.; Huang, Y.; Cai, Z.; Zhou, L.; Xing, Z.; Wang, H. Study on preparation and wear resistance of NiCrBSi-WC/Co composite coatings by pulsed magnetic field assisted supersonic plasma spraying. *Surf. Coat. Technol.* **2022**, *448*, 128897. [[CrossRef](#)]
13. Fals, H.; Aguiar, D.; Fanton, L.; Belem, M.; Lima, C. A new approach of abrasive wear performance of flame sprayed NiCrSiBFeC/SiC composite coating. *Wear* **2021**, *477*, 203887. [[CrossRef](#)]
14. Ping, X.; Sun, S.; Wang, F.; Fu, H.; Lin, J.; Lei, Y. Effect of Cr₃C₂ addition on the microstructure and properties of laser cladding NiCrBSi coatings. *Surf. Rev. Lett.* **2019**, *26*, 1850207. [[CrossRef](#)]
15. Bedmar, J.; de la Pezuela, J.; Riquelme, A.; Torres, B.; Rams, J. Impact of Remelting in the Microstructure and Corrosion Properties of the Ti6Al4V Fabricated by Selective Laser Melting. *Coatings* **2022**, *12*, 284. [[CrossRef](#)]
16. Bergant, Z.; Grum, J. Quality improvement of flame sprayed, heat treated and remelted NiCrBSi coatings. *J. Therm. Spray Technol.* **2009**, *18*, 380–391. [[CrossRef](#)]
17. Dong, T.; Liu, L.; Wang, R.; Yuan, J.; Feng, Y. Effect of induction remelting on microstructure and wear resistance of plasma sprayed NiCrBSiNb coatings. *Surf. Coat. Technol.* **2019**, *364*, 347–357. [[CrossRef](#)]
18. Torkashvand, K.; Gupta, M.; Bjorklund, S.; Joshi, S. Tribological Performance of Thin HVAF-Sprayed WC-CoCr Coatings Fabricated Employing Fine Powder Feedstock. *J. Therm. Spray Technol.* **2023**, *32*, 1033–1046. [[CrossRef](#)]
19. Thakur, L.; Vasudev, H. *Thermal Spray Coatings*; CRC Press: Boca Raton, FL, USA, 2021.
20. Kroemmer, M. *Praxis des Thermischen Spritzen*; Thiebes Druck GmbH: Düsseldorf, Germany, 2014.

21. Shahsavari, M.; Imani, A.; Setavoraphan, A.; Schaller, R.F.; Asselin, E. Electron beam surface remelting enhanced corrosion resistance of additively manufactured Ti-6Al-4V as a potential in-situ re-finishing technique. *Sci. Rep.* **2022**, *12*, 11589. [[CrossRef](#)] [[PubMed](#)]
22. Mehdizadeh, M. *Microwave/RF Applicators and Probes for Material Heating, Sensing, and Plasma Generation*; William Andrew: London, UK, 2015.
23. Sang, P.; Chen, L.-Y.; Zhao, C.; Wang, Z.-X.; Wang, H.; Lu, S.; Song, D.; Xu, J.-H.; Zhang, L.-C. Particle Size-Dependent Microstructure, Hardness and Electrochemical Corrosion Behavior of Atmospheric Plasma Sprayed NiCrBSi Coatings. *Metals* **2019**, *9*, 1342. [[CrossRef](#)]
24. Dai, L.; Chan, Y.; Vastola, G.; Khan, N.; Raghavan, S.; Zhang, Y. Characterizing the intrinsic properties of powder—A combined discrete element analysis and Hall flowmeter testing study. *Adv. Powder Technol.* **2021**, *32*, 80–87. [[CrossRef](#)]
25. Kandevara, M.; Kalitchin, Z.; Stoyanova, Y. Influence of Chromium Concentration on the Abrasive Wear of Ni-Cr-B-Si Coatings Applied by Supersonic Flame Jet (HVOF). *Metals* **2021**, *11*, 915. [[CrossRef](#)]
26. Kocaman, E.; Kilinc, B.; Durmaz, M.; Sen, S.; Sen, U. The influence of chromium content on wear and corrosion behavior of surface alloyed steel with $\text{Fe}_{(16-x)}\text{Cr}_x(\text{B,C})_4$ electrode. *Eng. Sci. Technol. Int. J.* **2021**, *24*, 533–542. [[CrossRef](#)]
27. Azzoug, R.; Mebdoua, Y.; Hellal, F.; Marra, F. Analysis of microstructure, mechanical indentation and corrosive behavior of a thermally sprayed NiFeCrBSi-WC composite coating. *J. Alloys Compd.* **2022**, *900*, 163505. [[CrossRef](#)]
28. Liyanage, T.; Fisher, G.; Gerlich, A. Influence of alloy chemistry on microstructure and properties in NiCrBSi overlay coatings deposited by plasma transferred arc welding (PTAW). *Surf. Coat. Technol.* **2010**, *205*, 759–765. [[CrossRef](#)]
29. Valean, P.C.; Kazamer, N.; Pascal, D.T.; Muntean, R.; Barányi, I.; Marginean, G.; Serban, V.A. Characteristics of Thermally Sprayed NiCrBSi Coatings before and after Electromagnetic Induction Remelting Process. *Acta Polytech. Hung.* **2019**, *16*, 7–18.
30. *ASTM E1920-03*; Standard Guide for Metallographic Preparation of Thermal Sprayed Coatings. ASTM International: West Conshohocken, PA, USA, 2021.
31. *ASTM G99-17*; Standard Test Method for Wear Testing with a Pin-on-Disk Apparatus. ASTM International: West Conshohocken, PA, USA, 2017.
32. Archard, J. Contact and rubbing of Flat Surfaces. *J. App. Phys.* **1953**, *24*, 981–988. [[CrossRef](#)]
33. Zhang, L.; Liao, X.-J.; Luo, X.-T.; Li, C.-J. Effect of Powder Particle Size and Spray Parameters on the Ni/Al Reaction During Plasma Spraying of Ni-Al Composite Powders. *J. Therm. Spray Technol.* **2021**, *30*, 181–195. [[CrossRef](#)]
34. Fauchais, P.; Montavon, G.; Bertrand, G. From Powders to Thermally Sprayed Coatings. *J. Therm. Spray Technol.* **2010**, *19*, 59–80. [[CrossRef](#)]
35. Larsson, M. Introduction to a new standardized test method for mixes, the Gustavsson flowmeter funnel. In Proceedings of the International Powder Metallurgy Congress and Exhibition, EURO PM 2013, Gothenburg, Sweden, 5–18 September 2013.
36. *ASTM B212-21*; Standard Test Method for Apparent Density of Free-Flowing Metal Powders Using the Hall Flowmeter Funnel. ASTM International: West Conshohocken, PA, USA, 2021.
37. Lu, H.; Gou, X.; Liu, Y.; Gong, X. Effect of Particle Size on Flow Mode and Flow Characteristics of Pulverized Coal. *Powder Part. J.* **2015**, *32*, 143–153. [[CrossRef](#)]
38. Karimi, M.; Salimijazi, H.; Golozar, M. Effects of remelting processes on porosity of NiCrBSi flame sprayed coatings. *Surf. Eng.* **2016**, *32*, 238–243. [[CrossRef](#)]
39. Liu, X.; Lin, M.; Yang, S.; Ruan, J.; Wang, C. Experimental Investigation of Phase Equilibria in the Ni-Cr-Si Ternary System. *J. Phase Equilibria Diffus.* **2014**, *35*, 334–342. [[CrossRef](#)]
40. Yuan, L.; Wang, H. Corrosion behavior of a γ -toughened $\text{Cr}_{13}\text{Ni}_5\text{Si}_2/\text{Cr}_3\text{Ni}_5\text{Si}_2$ multi-phase ternary metal silicide alloy in NaCl solution. *Electrochim. Acta* **2008**, *54*, 421–429. [[CrossRef](#)]
41. *ASTM E2109-01*; Standard Test Methods for Determining Area Percentage Porosity in Thermal Sprayed Coatings. ASTM: West Conshohocken, PA, USA, 2021.

Disclaimer/Publisher’s Note: The statements, opinions and data contained in all publications are solely those of the individual author(s) and contributor(s) and not of MDPI and/or the editor(s). MDPI and/or the editor(s) disclaim responsibility for any injury to people or property resulting from any ideas, methods, instructions or products referred to in the content.